Engineering Geology 139–140 (2012) 28–37

Contents lists available at SciVerse ScienceDirect

Engineering Geology

journal homepage: www.elsevier.com/locate/enggeo

Microstructure, porosity and mineralogy around fractures in Olkiluoto bedrock

Jukka Kuva [a,*], Marja Siitari-Kauppi [b], Antero Lindberg [c], Ismo Aaltonen [d], Tuomas Turpeinen [a], Markko Myllys [a], Jussi Timonen [a]

[a] University of Jyväskylä, Department of Physics, Survontie 9, 40500 Jyväskylä, Finland
[b] University of Helsinki, Laboratory of Radiochemistry, A.I. Virtasen aukio 1, 00014 Helsingin Yliopisto, Finland
[c] Geological Survey of Finland, Betonimiehenkuja 4, 02151 Espoo, Finland
[d] Posiva Oy, Olkiluoto, 27160 Eurajoki, Finland

ARTICLE INFO

Article history:
Received 28 November 2011
Received in revised form 29 March 2012
Accepted 12 April 2012
Available online 27 April 2012

Keywords:
Computed X-ray tomography
Petrography
C-14-PMMA method
Porosity analysis
3D structure analysis
Water-conducting fractures

ABSTRACT

3D distributions of minerals and porosities were determined for rock-core samples that included water-conducting fractures. The analysis of these samples was performed using conventional petrography methods, C-14-PMMA porosity analysis and X-ray tomography. It seems that the properties of rock around a water-conducting fracture depend on so many uncorrelated factors that no clear pattern emerged even for rock samples with a given type of fracture. We can conclude, however, that the present combination of methods can be used to infer novel structural information about alteration zones adjacent to fracture surfaces.

1. Introduction

Unraveling the effect on the surrounding rock matrix of water flowing in open fractures is important for understanding the basic mechanisms of rock alteration. Alteration is known to be a complex process: a combination of physical and chemical changes in rock texture, structure, and element composition, which often lead to increased porosity and formation of fractures and fissures. Chemical alteration includes dissolution of mineral elements followed by precipitation of some of the dissolved elements. Finally new mineral phases, in most cases clays, are formed with a structure that differs from that of the unaltered rock (Velde and Meunier, 2008; Rossi and Graham, 2010). Such changes in the physical and chemical properties of rock adjacent to open fractures affect the migration properties of solutes present in the groundwater that flows in these fractures. So as to investigate if there are generic changes that could be classified with respect to the pore structure in the rock adjacent to water-conducting fractures, we analyzed drill-core samples from Olkiluoto, Finland.

In the Olkiluoto bedrock, fractures are typically dominated by calcite, hydrothermal clays, or both. Many fractures are actually single faults and have slickensided surfaces. The calcite is often in the core of the fracture filling system and is generally part of the latest filling phases. It is found even in non-cohesive clays as a 'glue' between clay particles. Calcite and sulfides usually occur together on surfaces of hydrothermal clay minerals. In assemblages of illite and kaolinite, kaolinite seems to be the youngest component and is located in the core of the fracture infill. In fractures where illite is the dominating phase, it usually lines the fracture walls, whereas kaolinite typically forms an incohesive filling.

Based on the typical fracture characteristics in Olkiluoto, three fracture types were selected for this study: calcite dominated fractures, clay dominated fractures, and slickensided fractures. The mineralogical and porosity changes, and other characteristic properties, of twelve drill-core samples were studied near fracture surfaces by the C-14-PMMA method, X-ray tomography, and optical microscopy.

Based on visual observations and the results of the above methods, there indeed appeared rock properties in the vicinity of fractures that had been water conducting, which were different from those in the host rock. Based on conceptual understanding of the geological processes at Olkiluoto, these fracture-induced changes in the rock texture could be linked to fracture evolution and hydrothermal alteration of the rock (Aaltonen et al., 2010; Posiva, 2011).

* Corresponding author at: University of Jyväskylä, Department of Physics, PL 35, 40014 Jyväskylän Yliopisto, Finland. Tel.: +358 503759567.
E-mail addresses: jukka.kuva@iki.fi (J. Kuva), marja.siitari-kauppi@helsinki.fi (M. Siitari-Kauppi), antero.lindberg@gtk.fi (A. Lindberg), ismo.aaltonen@posiva.fi (I. Aaltonen), tuomas.turpeinen@jyu.fi (T. Turpeinen), markko.myllys@jyu.fi (M. Myllys), jussi.timonen@phys.jyu.fi (J. Timonen).

0013-7952/$ – see front matter © 2012 Elsevier B.V. All rights reserved.
doi:10.1016/j.enggeo.2012.04.008

2. Methods and samples

2.1. X-ray tomography

Computed tomography (CT) is an imaging method where cross-sectional images of a sample can be reconstructed from the transmission ('shadowgrams') or diffracted data collected by illuminating the sample from many different directions (Wellington and Vinegar, 1987; Cnudde et al., 2006). Computed X-ray tomography (CT) with laboratory scale equipment (microtomography, μCT) is typically based on attenuation of X-rays.

The finite spot size of the X-ray source limits the resolution of μCT devices, being typically a few micrometers, and about a μm at best. In conventional absorptive-contrast imaging, the Feldkamp algorithm (Feldkamp et al., 1984) is usually used, and it assumes pure absorption of monochromatic X-rays, while the spectrum produced by an X-ray tube is non-monochromatic, which produces artifacts in the reconstructed images of high-density samples. Using high energies and proper filters during imaging, these artifacts can be minimized. In the case of non-monochromatic X-rays, the attenuation coefficient is proportional to the effective atomic number and density of the matter, and should be integrated over the X-ray energies used in the imaging. The reconstructed images can thus be interpreted as 3D distributions of a scaled attenuation coefficient integrated over the X-ray energies used.

The experiments described in this paper were done with a SkyScan 1172 desktop scanner and an Xradia Micro-XCT-400 scanner. With the SkyScan device, samples were scanned using exposure times of 5301–10,013 ms with an acceleration voltage of 100 kV and a power of 10 W. The rotation step was 0.3° and every shadowgram was an average over 10 frames. The voxel size was 5.8–8.6 μm in the large subsamples and 1.7–2.0 μm in the small subsamples. With the Xradia device samples were scanned using exposure times of 21–30 s with an acceleration voltage of 90 kV and a power of 7.92 W. The rotation step was 0.3 or 0.33° depending on the sample, the distance between the source and sample was 50–70 mm, the distance between the detector and sample was 5.0–8.5 mm, and the resulting voxel size was 2.98–3.15 μm. In all cases the details resolved were close to, but a bit larger, than the voxel sizes.

2.2. Analysis and visualization

The 3D tomographic data were first filtered for noise with an algorithm described in Appendix B. A gray-scale-based mineral analysis of the resulting data was then done in 2D using ImageJ, an open-source image-processing and analysis software for multiple platforms. The gray-scale values of the images were divided into different intervals (mineral components) by manual thresholding. The threshold values that separated different components were estimated visually by comparing the segmentation result with the unsegmented cross section, and also from the gray-scale histograms by fitting a normal or log-normal distribution to each peak of the histogram and using the intersections of these distributions. The abundances of the mineral components were determined as the numbers of voxels that belonged to the segmented regions. In order to compare the gray-scale values in the image to those in other tomographic images, one has to calibrate the gray-scale values by imaging phantoms of known minerals along with the sample. This technique was tried out as part of the study, and a description of the results achieved is given in Appendix A.

So as to determine the distributions of the mineral components as a function of distance to the fracture, the tomographic reconstruction of each sample was divided into stacks of the shape of the fracture surface as shown in Fig. 1, and the mineral composition of each stack was analyzed separately. To achieve this, the surface of the sample was first determined with an algorithm (Chinga-Carrasco et al., 2008) that forced a dynamic 3D interface to approach the surface until it reached force equilibrium with the gray-scale values of the image voxels that provided an opposing force to the interface motion. An image stack was then formed such that the shape of the slices was the same as that of the identified surface. The distributions determined were not quite accurate because every data point in the

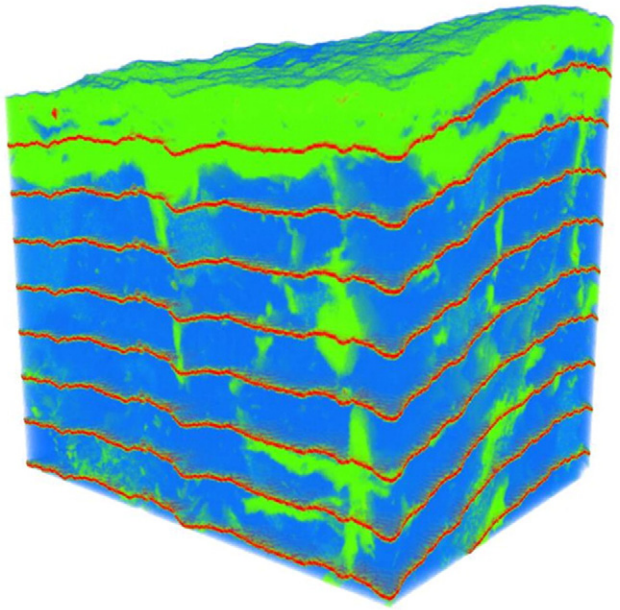

Fig. 1. Division of a sample into surface-shaped stacks for the analysis of the distribution of mineral components as a function of distance to the fracture, here at the top of the image.

Fig. 2. The two halves of sample OL_KR13_171.55.